

The alginate dialdehyde crosslinking on curcumin-loaded zein nanofibers for controllable release



Jiawen Li^a, Yuanhao Zheng^a, Peng Wang^{b,*}, Hui Zhang^{a,c,*}

^a College of Biosystems Engineering and Food Science, Zhejiang Key Laboratory for Agro-Food Processing, Zhejiang University, Hangzhou 310058, China

^b College of Food and Health, Zhejiang Agriculture and Forestry University, Hangzhou 311300, China

^c Innovation Center of Yangtze River Delta, Zhejiang University, Jiaxing 314102, China

ARTICLE INFO

Keywords:

Electrospinning
Zein
Alginate dialdehyde
Crosslinking
Curcumin

ABSTRACT

In this study, electrospun zein/alginate dialdehyde (AD) nanofibers were prepared by green crosslinking. The degree of crosslinking could reach 50.72 %, and the diameter of electrospun fibers ranged from 446.2 to 541.8 nm. The generation of AD and the bonding of crosslinking were further confirmed by the changes on characteristic peaks and conformational ratios in the infrared spectroscopy and secondary structure analysis. High concentrations of AD led to improved thermal stabilities, mechanical properties, and hydrophobicity. And the highly crosslinked nanofibers (Z-8) owned the highest elastic modulus (24.92 MPa), tensile strength (0.28 MPa), and elongation at break (8.14 %) among five samples. Moreover, Z-8 possessed a high swelling ratio of 5.45 g/g, and a low weight loss of 6.09 %. The samples could encapsulate curcumin efficiently and show controllable release behaviors based on different AD addition. And the oxidation resistance of nanofibers gradually improved, consistent with the release performances. This study indicated AD crosslinking favored the preparation and application of zein nanofibers, and the oxidized polysaccharide acted as the green crosslinking agent, which provided reference value for the application of polysaccharides in food-related electrospun materials.

1. Introduction

As a feasible and multifunctional technique for constructing nano-scale polymeric fiber systems, the electrospinning of polymers has dragged great attention in recent years. The highly porous three-dimensional network, high specific surface area, and high porosity with tunable microstructures make the nanofiber materials promising in tremendous applications in different fields (e.g., drug delivery, food packaging, filtration and adsorption) (Aydin et al., 2022; Mendes, Stephanten, & Chronakis, 2017; Topal et al., 2022). Diverse parameters modulate the fiber diameter and the resulting properties during the electrospinning process, which might influence the sustained or controlled release behaviors. In addition to the operating conditions like concentration, voltage, flow rate, temperature, humidity, etc., the basic parameters of the raw materials play an important role in the performance of nanofibers. For instance, the molecular weight, molecular structure, and chain length of polymers affect the suitability for electrospinning, which indirectly limit the application of some polymer materials (Laha, Sharma, & Majumdar, 2017; Wang et al., 2022).

For most food-related and biomedical applications, the complete

usage of biopolymers in electrospinning would be a simple and ideal strategy. The obtained nanofibers could be biodegradable, environmentally friendly, and even edible. Such materials can be utilized in food packaging and storage, nutrition delivery, and food quality monitoring (Yao, Gao, Chen, & Xia, 2021). Some biopolymers (e.g., gelatin or pullulan) have a strong spinnability so that they can be electrospun individually. But more types of biopolymers, especially polysaccharides, can only form electrospun nanofibers by blending or other indirect methods. Otherwise, nanofibers with uniform and stable structures could not be obtained (Mendes et al., 2017). Besides, compared with inorganic and synthetic polymer materials, biopolymer nanofibers always present a weaker physical property and higher hydrophilicity, which are not conducive to real applications (Li & Zhang, 2023). For this reason, it is meaningful to further strengthen the pure biopolymer structure by crosslinking, and various kinds of crosslinking strategies have been conducted to improve the performance of biopolymer systems. Laha et al. (2017) developed electrospun gelatin nanofibers for the controlled and sustainable release of piperine. They demonstrated that the glutaraldehyde-crosslinked nanofiber mesh exhibited better controllable release behaviors, with the flexibility to alter loading

* Corresponding authors.

E-mail addresses: wpeng@zafu.edu.cn (P. Wang), hubert0513@zju.edu.cn (H. Zhang).

abilities as per therapeutic conditions. Pereira et al. (2023) studied the effect of ultraviolet radiation on soy protein isolated electrospun mats, where the radiation was demonstrated to be a simple and effective method for sterilizing nanofibers under the studied conditions. Meanwhile, the green crosslinking strategy is expected where the raw materials including crosslinkers could be obtained from natural resources easily, and the formula may enable more biopolymers to be utilized.

Alginate, an important naturally existing polysaccharide, has been studied widely in various fields, which shows a great potential in fabricating structural materials like functional hydrogels (Mendes et al., 2017). Due to its rigid and extended structure, the electrospinning of alginate is still challenging. And alginate dialdehyde (AD) is one of the effective crosslinking reagents where alginate was oxidized with periodate, leading to the formation of dialdehyde groups. To be specific, the aldehyde groups could crosslink with the amine groups of protein by Schiff-base reaction, which has been extensively utilized in biomedicine for the delivery of drugs and biomolecules. It was proved that the effect of AD on mechanical strength was close to glutaraldehyde and notably superior to poly epoxy (Xu et al., 2013). Therefore, applying the oxidized products would be a feasible way to involve alginate in electrospun biopolymers. And the addition of AD could be expected to efficiently crosslink the protein, and further improve the physiochemical properties of the nanofibers. After loading bioactive compounds, the AD crosslinking may also be conducive to modulating the encapsulation efficiency and release behaviors of the nanofiber materials.

In this study, AD was first prepared, then used to crosslink the electrospun zein nanofibers with different degrees. Zein was selected as the protein with a good spinnability to react with AD. It was hypothesized that Schiff base bonding caused by AD-crosslinking could improve the physical properties of the fiber membranes, and favor the loading and delivery of curcumin (CUR). The solutions for electrospinning were evaluated by enzyme-linked immunosorbent assay, rheology, and electrical conductivity. The characterizations of the fibers were conducted via the following investigations: field-emission scanning electronic microscopy, differential scanning calorimetry, thermogravimetric analysis, Fourier transform infrared spectroscopy, mechanical properties, water contact angle measurements, and swelling behaviors. Eventually, the encapsulation and *in vitro* release behaviors of CUR were investigated, and the oxidation resistance of samples was determined.

2. Experimental

2.1. Materials

Sodium alginate (SA, CP, viscosity = 100—200 mPa·s; molecular weight = 398.31 Da; M/G = 1.1), sodium periodate, 1,1-Diphenyl-2-picrylhydrazyl radical (DPPH), and 2,2'-azinobis-(3-ethylbenzthiazoline-6-sulphonate) (ABTS) were purchased from Aladdin, Inc. (Shanghai, China). Ninyhydrin was purchased from Shanghai Yuanye Bio-Technology Co., Ltd. (China). Xylene brilliant cyaninG was obtained from Nanjing Jiancheng Bio-Technology Co., Ltd. (China). Curcumin (CUR) and zein were supplied by Macklin Reagent Co., Ltd. (Shanghai, China). Other reagents were obtained from Sinopharm Chemical Reagent Co., Ltd. (Shanghai, China).

2.2. Fabrication and characterization of alginate dialdehyde (AD)

SA (5 g) was dissolved in 200 ml distilled water and 50 ml ethanol, then sodium periodate with an equal mole of the monomeric unit of SA was added into the solution and stirred in darkness for reaction. Subsequently, 10 ml ethylene glycol was mixed with the reaction solution for 1 h, and the product was purified by precipitation with the addition of sodium chloride (5 g) and ethanol (900 ml). Finally, the solution was dialyzed (molecular weight cut off: 3500 Da) with ultrapure water and lyophilized. The oxidation degree and dialdehyde content were determined by iodometric titration and hydroxylamine hydrochloride

titration, respectively. The molecular weights of AD were estimated using gel permeation chromatography (GPC, Agilent PL-GPC50, USA).

2.3. Preparation of solutions for electrospinning

The spinning solutions were prepared by dissolving 27 % (w/v) zein in 75 % (v/v) ethanol aqueous solution without and adding 2 %, 4 %, 6 %, and 8 % AD with respect to the protein weight, which were denoted as Z-0, Z-2, Z-4, Z-6, and Z-8, respectively. CUR was then added into the solutions (2 % w/w of the protein content), which were stirred at 25 °C for 2 h for further characterizations and electrospinning.

The apparent viscosity was evaluated using the stress-controlled rheometer (MCR 302, Anton Paar, Austria). The shear rate was set as 100 s⁻¹ with a temperature of 20 °C throughout the test. The conductivity was measured at 20 °C using a conductivity meter (DDS-307, Shanghai Precision & Scientific Instrument Co., Ltd, China).

2.4. Crosslinking degree

A ninhydrin assay was used to evaluate the crosslinking degree of samples. The concentration of free amino groups in solutions was detected with enzyme-linked immunosorbent assay (ELISA) reader colorimetry (Shanghai Yuanye Bio-Technology, China) according to the manufacturer instructions, and then determined at the optical absorbance of 570 nm (Tecan Infinite M200, Mannedorf, Switzerland). The crosslinking degree was determined by following the equation:

$$\text{Crosslinking degree}(\%) = \frac{A_i - A_f}{A_i} \times 100 \quad (1)$$

where A_i and A_f are the absorbances of the non-crosslinked and cross-linked samples, respectively, which also represent the mole fractions of free NH₂ remaining in the samples.

2.5. Electrospinning

By using an integrated electrospinning machine (YFSP-T, Tianjin Yunfan Technology Co., Ltd, China), electrospinning of the solutions was performed at a rate of 0.5 ml/h and a voltage of 17.0 kV, and the distance between the collector and needle tip (internal diameter: 0.61 mm) was 10.0 cm. The solutions were placed into syringes (5 ml) and squeezed using a syringe pump. The temperature and humidity were conducted at 25 °C and 40 %, respectively. Nanofibers were obtained on a rotating cylindrical collector at a speed of 260 rpm. After 8 h, a piece of nanofiber film of around 30 × 20 cm could be obtained.

2.6. Morphology

The surface morphology was examined by applying Field-emission scanning electron microscopy (FE-SEM). The Au/Pd mixture was sputtered on the film pieces of nanofibers, which were then examined in the microscope (Hitachi, SU8010, Japan) at room temperature.

2.7. Thermal analysis

A thermogravimetric analyzer (TGA; TA Instruments, TA Q500, USA) was conducted to measure the thermal weight loss of the films with a temperature range of 50 to 600 °C with a heating speed of 10 °C/min under a N₂ atmosphere.

Thermal characterization of the films was investigated by differential scanning calorimetry (DSC; TA Instruments Q200, USA). Approximately 5 mg of films were heated at the temperature ranged between 25 and 300 °C with a heating rate of 10 °C/min, under the N₂ atmosphere.

2.8. Fourier transform infrared spectra (FTIR)

The spectra analysis was performed on the tablets containing 3 mg films and approximately 100 mg potassium bromide using FTIR spectrometer (Nicolet iS50, Thermo Scientific, USA). The FTIR spectra were recorded in the range of 4000—400 cm⁻¹ and at a resolution of 4 cm⁻¹. The spectra plots represented the average of 32 scans.

2.9. Mechanical tests

To conduct the mechanical tests, the nanofibers were tested on a dynamic thermal mechanical analysis instrument (DMA, TAQ800, TA, USA) loaded with a maximum force of 18 N. The nanofiber films were cut in the shape of 4 cm × 1 cm and immobilized for the tensile test. The film thickness was determined via a spiral micrometer to calculate the stress and strain. The tensile speed was conducted to 2 mm/min. The humidity and temperature were kept at 35 % and 30 °C, respectively. According to the obtained stress-strain curves, the tensile strength, elastic modulus, and elongation at break were determined.

2.10. Water contact angle (WCA)

Using the contact angle meter (OCA 20, Data Physics Co. Ltd., Germany), a droplet of deionized water was slowly added to the surface of electrospun films with a camera for recording (room temperature). Both the WCA of the right side and left side were measured and averaged. According to the obtained pictures (at 0 and 10 s, respectively), WCA values were recorded from five measurements at different positions of the same sample.

2.11. Water stability

The water stability test was conducted based on the study of Deng et al. (2018). The electrospun films were cut into pieces of around 10 mg, which were immersed in 10 ml of sodium phosphate buffer (PBS, pH = 7.4) for 25 h at room temperature. The wet film pieces were then taken out and dried under vacuum, and the micromorphology of the obtained samples was observed by FE-SEM micrographs. The swelling ratio and weight loss were determined using the equations below:

$$\text{Swelling ratio (\%)} = \frac{M_1 - M_0}{M_0} \times 100 \quad (2)$$

$$\text{Weight loss (\%)} = \frac{M_0 - M_2}{M_0} \times 100 \quad (3)$$

where M_0 represents the initial weight before 24 h immersion, M_1 denotes the weight of the swelling sample, and M_2 represents the final weight of the dried sample.

2.12. Release of CUR and encapsulation efficiency

The CUR released was evaluated by the method of Wang, Li, Zhang, Feng, and Zhang (2020). 5 mg of the sample was added in 5 ml 0.01 M PBS (pH = 7.4) with 0.05 % w/v Tween 80, which was used to promote the CUR release. The mixture was stirred at 200 rpm throughout the test. At predetermined time intervals, 100 µl of the solution was withdrawn and replaced with 100 µl solvent, whose absorbance was detected at 435 nm.

The encapsulation efficiency was determined based on Zhang et al. (2019) with modifications. 5 mg of the sample was mixed with 5 ml ethanol aqueous solution (50 % v/v), which was stirred at 100 rpm for 15 min (IKA, Germany) until the sample was completely dissolved. Still, the absorbance was determined at 435 nm. The cumulative CUR release and encapsulation efficiency were evaluated by the equations:

$$\text{CUR release (\%)} = \frac{M_t}{M_\infty} \times 100 \quad (4)$$

$$\text{Encapsulation efficiency (\%)} = \frac{M_r}{M_\infty} \times 100 \quad (5)$$

where M_t denotes the amount of CUR released at the specific time, M_∞ is the CUR amount initially added in the electrospun fibers, and M_r relates to the measured curcumin amount in the samples. By preparing a series of CUR solutions with gradient concentrations, a standard curve was made to determine the concentration of the sample. The temperature was kept at 25 °C throughout the experiments above.

To further evaluate the *in vitro* release characteristic of CUR, four different models were applied to fit the obtained release data (Lertpaiprod & Tiyaboonchai, 2022). The Zero-order, First-order, Higuchi, and Korsmeyer-Peppas models were given in the following equations:

$$\frac{M_t}{M_\infty} = kt \quad (6)$$

$$\ln \frac{M_t}{M_\infty} = kt \quad (7)$$

$$\frac{M_t}{M_\infty} = kt^{0.5} \quad (8)$$

$$\frac{M_t}{M_\infty} = kt^n \quad (9)$$

Where M_t/M_∞ denotes the release ratio of CUR at time t , k represents the release constant of different models, and n relates to the release exponent. Moreover, the best fitting model was determined from the coefficient of determination (R^2).

2.13. Antioxidant activity

The ABTS and DPPH scavenging activities were conducted according to Wang et al. (2022) with modifications. 5 mg sample was mixed with 5 ml PBS solution (pH = 7.4), 0.05 % w/v Tween 80, and stirred at 200 rpm, room temperature. The ABTS solution (7.4 mM) was prepared and placed in darkness for 24 h. When the absorbance of the solution was 0.70 ± 0.05 at 734 nm, 200 µl sample solution was added into 2 ml ABTS solution for reaction (6 min), room temperature. After the incubation, the absorbance was recorded at 734 nm.

For the DPPH radical scavenging assay, 5 mg of sample was mixed with 5 ml PBS solution (pH = 7.4), 0.05 % w/v Tween 80, and stirred at 200 rpm, room temperature. At regular intervals, 100 µl mixture was taken and reacted with isochoric DPPH solution (0.2 mM in 95 % v/v ethanol aqueous solution). After the incubation in darkness for 30 min, the absorbance was read at 517 nm.

The ABTS and DPPH radical scavenging activities were evaluated based on the following equations:

$$\text{ABTS radical scavenging activity (\%)} = \frac{A_0 - A_1}{A_0} \times 100 \quad (10)$$

$$\text{DPPH radical scavenging activity (\%)} = \frac{A_2 - A_3}{A_2} \times 100 \quad (11)$$

where A_0 and A_1 denote the absorbance of the control and the absorbance of sample in ABTS radical scavenging assay, respectively. A_2 and A_3 relate to the absorbance of the control and the absorbance of the sample in the DPPH radical scavenging assay, respectively.

2.14. Statistical analysis

Results were obtained by applying Origin 2023 software, and the statistically significant differences were determined by the one-way ANOVA and post hoc Tukey's multiple comparisons as post-test, $P <$

Table 1

Properties of the electrospinning solutions.

Sample	Crosslinking degree (%)	Viscosity (mPa·s)	Conductivity (uS/cm)
Z-0	/	115.75 ± 4.19 ^e	94.00 ± 6.08 ^b
Z-2	23.03 ± 8.50 ^c	145.00 ± 1.73 ^d	144.23 ± 4.04 ^a
Z-4	30.63 ± 7.57 ^{bc}	189.00 ± 16.04 ^c	144.29 ± 1.53 ^a
Z-6	46.36 ± 1.96 ^b	236.00 ± 12.73 ^b	145.38 ± 2.52 ^a
Z-8	50.72 ± 3.36 ^a	288.50 ± 10.61 ^a	147.33 ± 3.21 ^a

Different letters in the same column represented significant differences ($P < 0.05$).

0.05. The data were calculated from at least three repeated measurements, and displayed as mean ± standard deviation.

3. Results and discussion

3.1. Properties of the electrospinning solutions

The molecular weight, oxidation degree, and dialdehyde content of AD were 216.03 Da, 47.24 %, and 5.27 mmol/g, respectively. Hydroxyl groups on C2 and C3 of the repetitive unit of SA were oxidized by sodium periodate to create aldehyde groups, which enabled AD to crosslink with the amino groups of zein (Ding, Zhou, Zeng, Wang, & Shi, 2017). And the crosslinking degree, viscosity, and conductivity of the electrospinning solutions were shown in Table 1. The extent of crosslinking can be evaluated based on the loss of free amino groups of zein, and the crosslinking degree became higher with increasing AD addition (from 23.03 % to 50.72 %), where Z-8 owned the highest crosslinking degree. Results revealed that AD, within a certain concentration range, was able to crosslink zein effectively. This also confirmed the amino groups are involved as a highly nucleophilic agent in the crosslinking of the solutions indeed (Chetouani et al., 2022).

The viscosity and conductivity of spinning solutions were important factors affecting the extensibility and stretching of polymer chains during electrospinning, as well as the diameters of the obtained fibers. For the viscosity, the higher content of AD contributed to a higher viscosity significantly (from 115.75 to 288.50 mPa·s). Angarano et al.

(2013) also found a consistent effect of crosslinking on the apparent viscosity, where the slowly progressing crosslinking by glyoxal increased the viscosity of the gelatin solutions for electrospinning. For the conductivity, Z-0, the sample without AD, presented the lowest conductivity of 94.00 uS/cm, which could be improved by the addition of AD (up to 147.33 uS/cm). But the increasing addition of AD would not significantly change conductivity. Similarly, Jia et al. (2022) prepared pea protein isolate/pullulan spinning solutions with different amounts of glucose. 1.0 % of glucose significantly improved the conductivity while further addition did not favor the increase of conductivity. Zhao et al. (2022) prepared the keratin-based nanofiber membrane cross-linked by glutaraldehyde for 8 h where the treatment bared groups that absorb more electrolytes, resulting in a higher conductivity.

3.2. Micromorphology and fiber diameter

Although the zein molecules with globular conformation could not exhibit sufficient interchain associations or entanglements, the solutions were able to be electrospun by using alcohol-based solvents (75 % v/v ethanol) (López-Rubio & Lagaron, 2012). As shown in Fig. 1, all the fibers displayed a straight shape without beaded structures, which confirmed the extensive molecular entanglements in samples with different formulas (Drosou, Krokida, & Biliaderis, 2018). No obvious change in the fiber morphology was observed, demonstrating that adding AD would not lead to uneven fiber structures.

As for fiber diameter, with the increasing crosslinking degree, the fiber diameter decreased at first (from 541.8 to 446.2 nm) and then increased (up to 506.6 nm). Fiber diameter was strongly dependent on parameters like the solution properties, or operating conditions (applied voltage, flow rate, etc.). For the spinning solution, the increase in viscosity gave rise to a larger fiber diameter while the increasing conductivity caused higher elongation of the jet, resulting in a smaller fiber diameter (Deng et al., 2018). The process variables were the same throughout the electrospinning, so the changes in polymer solution properties may account for the trend in fiber diameter. Combining with the data in Table 1, the trend could be explained by that with the addition of AD, both the viscosity and conductivity increased. The conductivity was the main factor to decrease the fiber diameter at a

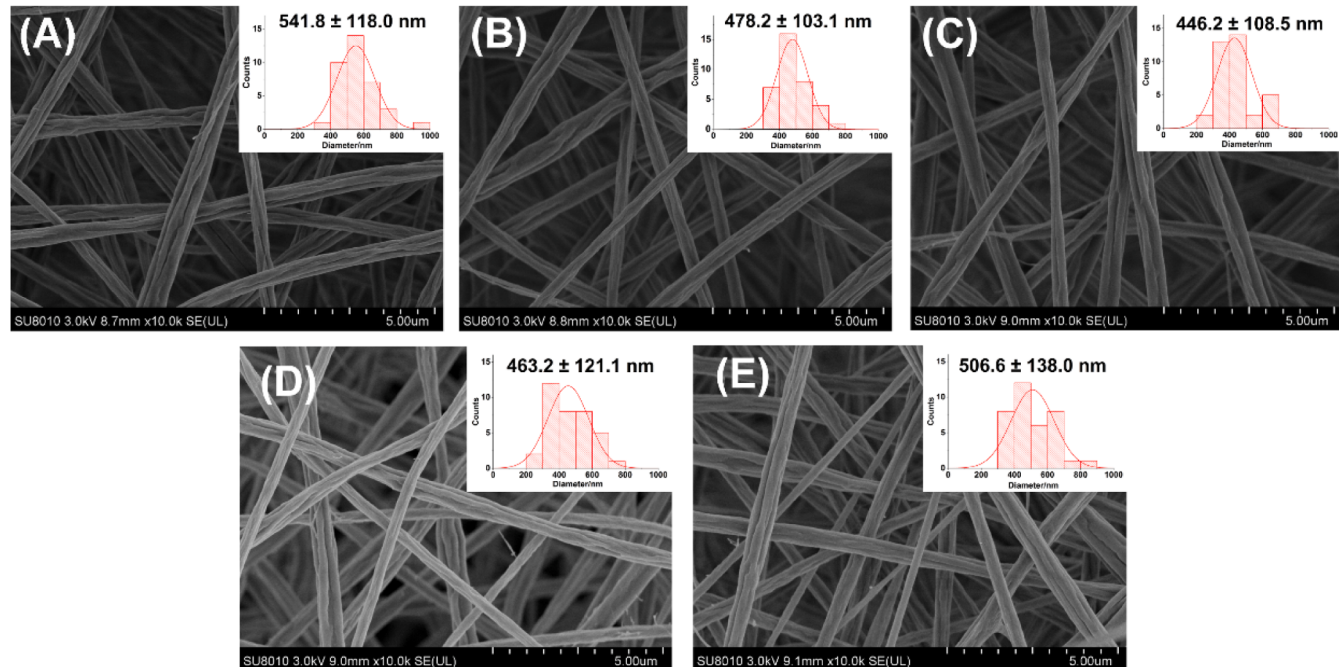


Fig. 1. FE-SEM micrographs and fiber diameters of electrospun fibers with different AD addition. (A) Z-0, (B) Z-2, (C) Z-4, (D) Z-6, and (E) Z-8.

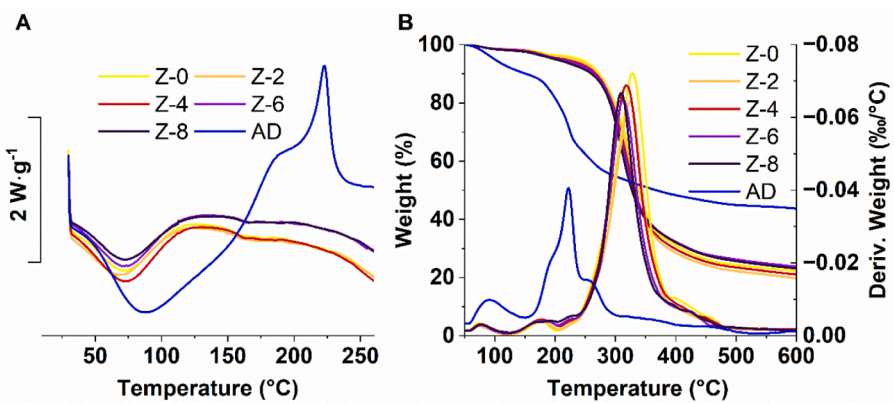


Fig. 2. (A) DSC curves and (B) TGA thermograms of the fibers and AD.

Table 2
DSC and TGA data of the fibers and AD.

Sample	DSC			TGA		
	Peak1 (°C)	ΔH_1 (J/ g)	Peak2 (°C)	ΔH_2 (J/g)	Peak (°C)	Residue (%)
Z-0	73.11	128.25	162.60	10.31	328.00	22.21
Z-2	70.77	125.47	162.93	9.59	324.45	19.71
Z-4	73.77	122.61	162.27	6.78	318.33	21.03
Z-6	75.11	121.20	165.44	5.20	312.57	23.72
Z-8	73.78	116.24	164.44	4.20	309.33	23.10
AD	88.91	440.05	/	/	222.29	43.70

lower AD addition while the viscosity affected the diameter more significantly at a higher AD addition. In similar studies, Ghasemi et al. (2023) found that 10 wt% of zein incorporation reduced the fiber diameter of electrospun polyhydroxy butyrate scaffolds from 894 to 531 nm, which might be conducive to bone tissue engineering applications. Hajjari, Golmakan, and Sharif (2023) developed zein/C-phycocyanin nanofibers by electrospinning, and all fibers had a tubular morphology with larger diameters by adding phycocyanin. Further characterizations demonstrated the potential of the composite edible films for medical/nonmedical applications. On the other hand, the lower fiber diameter corresponded to a higher specific surface area at the same content, which would be desirable for developing loading/delivery nano-materials. A certain amount of AD addition may favor the construction of nanofiber materials (Campiglio, Contessi Negrini, Fare, & Draghi, 2019).

3.3. Thermal analysis

DSC and TGA were examined to evaluate the thermal stability of the nanofibers and pure AD. As shown in Fig. 2A and Table 2, the first peak of AD was at 88.91 °C, quite different from the protein-based fibers. The peaks around 70–75 °C and 160–170 °C related to thermal denaturation and thermal degradation temperature point of zein, respectively, and no obvious trend was found on the peaks. Nevertheless, the denaturation enthalpy (ΔH_1) of the fibers decreased from 128.25 to 116.24 J/g, and the degradation enthalpy (ΔH_2) of degradation decreased from 10.31 to 4.20 J/g, indicating the chemical bonds formed by AD crosslinking weakened the resistance of the zein nanofibers to thermal denaturation and degradation to some extent. The hydrophilic groups involved in crosslinking could interfere with hydrophobic interactions and lead to the aggregation of the protein, which might account for the reduction of enthalpy (Li, Zhao, Zhu, & Zhang, 2023).

In TGA curves (Fig. 2B), three periods were involved in the decomposed process of fibers and AD. The first period (0–250 °C for fibers, and 0–100 °C for AD) was mainly related to moisture evaporation, where the weight loss was relatively slow. In the next period (250–350 °C for fibers, and 100–250 °C for AD), samples lost weight rapidly because of the biopolymer depolymerization. And the last period was explained by the carbonization of proteins or polysaccharides (Li, Zhang, Li, & Zhang, 2022). Overall, AD presented a faster decomposition process but had more residue than fibers. And crosslinking would not significantly influence the thermal decomposition stability of the fibers, according to the residues at 600 °C. When examining the rate curves (the relatively small peaks in the first period were not recorded), the peaks occurred earlier with the increasing degree of crosslinking, suggesting

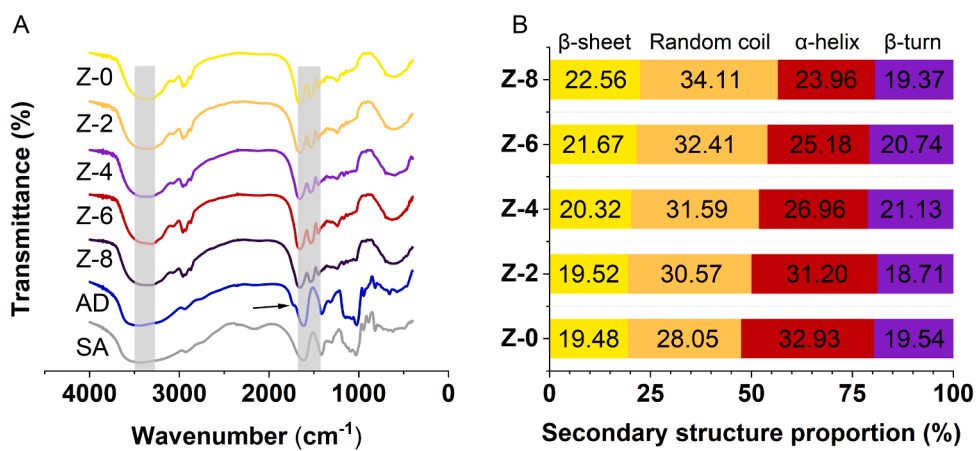


Fig. 3. (A) FTIR of the fibers, AD, and SA at 4000—400 cm^{-1} . (B) Secondary structure proportions of protein.

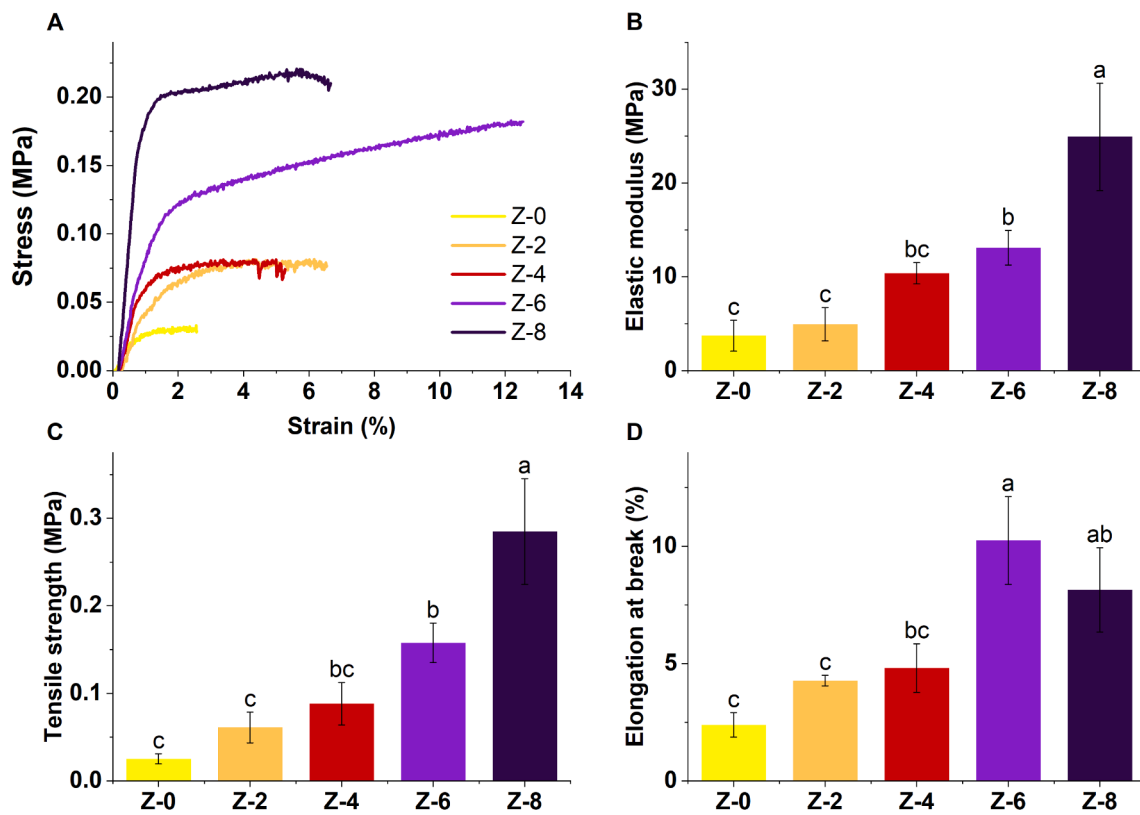


Fig. 4. Mechanical performances of nanofibers. (A) stress–strain curves, (B) elastic modulus, (C) tensile strength, and (D) elongation at break. Different letters in the same bar chart denoted significant differences ($P < 0.05$).

samples were more prone to mass decomposition in high temperatures. [Zhang, Wang, Li, Zhang, and Weiss \(2021\)](#) also fabricated gelatin composite nanofiber membranes with different crosslinking degrees, and genipin crosslinking could not improve thermal decomposition stability. Meanwhile, the fiber materials may be used for encapsulation or release, and the normal operating temperature was not high (below 100 °C). As the fibers lost weight no more than 10 % at 200 °C, the fibers exhibited high thermal stabilities on the whole, which was expected for practical applications ([Horuz & Belibagli, 2019](#)).

3.4. FTIR analysis

In the spectra of fibers, pure AD, and pure SA ([Fig. 3A](#)), the amide A band at around 3400 cm⁻¹ was assigned to N–H stretching of the amino groups in protein or O–H stretching. The amide I band at around 1600 cm⁻¹ and amide II band at around 1500 cm⁻¹ corresponded to C–O stretching and C–N stretching and bending, respectively ([Moreno, Orqueda, Gómez-Mascaraque, Isla, & López-Rubio, 2019](#)). By observing the curves of AD and SA, a small characteristic peak at 1734 cm⁻¹ was formed after the oxidation of SA, which related to C = O stretching and confirmed that SA was successfully transformed into AD. Moreover, after the addition of AD in zein, the newly formed peak disappeared, indicating the consumption of C = O by crosslinking. Furthermore, the quantitative analysis of the protein secondary structure was conducted by evaluating the FTIR curves at 1700—1600 cm⁻¹ and presented in [Fig. 3B](#). The conformational changes would significantly affect the spinnability of solutions and the morphology of nanofibers (e.g., the severely attenuated molecular entanglements among the polymeric chains might lead to breaking up of the jet, not conducive to electrospinning; a higher amount of β-sheet would impart a higher mechanical strength to the nanofibers) ([Drosou et al., 2018; Singh, Panda, & Pramanik, 2016](#)). To be specific, the content of α-helix decreased with the

increasing addition of AD, from 32.93 % to 23.96 %. By contrast, AD crosslinking caused higher content of β-sheet and random coil, from 19.48 % and 28.05 %, to 22.56 % and 34.11 %, respectively. Similarly, [Turasan, Barber, Malm, and Kokini \(2018\)](#) fabricated the casting zein films, and the glutaraldehyde crosslinking decreased the α-helix content but increased the β-sheet content statistically. And no significant difference was determined in the β-turn content. [Mattice and Marangoni \(2021\)](#) studied the zein networks crosslinked by microbial transglutaminase, and the crosslinked samples exhibited a notable increase in the contents of β-sheet and random coil while the content of α-helix had a significant decrease.

3.5. Mechanical properties

As shown in [Fig. 4A](#), the stress–strain curves could be mainly divided into two stages: the initial elastic stage and the following flat stage, indicating the start of structure fracture ([Li & Zhang, 2023](#)). On the whole, the films with a higher degree of crosslinking displayed a higher stress at the same strain, and Z-6 could be stretched to the longest length of its original shape. Z-8 possessed the highest elastic modulus (24.92 MPa), tensile strength (0.28 MPa), and elongation at break (8.14 %, no significant difference with Z-6) among the five samples, suggesting the best tensile mechanical character ([Fig. 4B, C, and D](#)). There was no significant difference in the three indexes between Z-0 and Z-2, indicating the low crosslinking degree did not affect the mechanical properties of films. On the other hand, the excessive addition of AD might result in an unexpected brittleness, and the films could not withstand a greater deformation. Various types of crosslinking reactions were proved to improve the mechanical properties, including carbohydrates and oxidized saccharides as crosslinking agents. For instance, [Jalaja and James \(2015\)](#) prepared the gelatin nanofiber films crosslinked by oxidized sucrose, which displayed enhanced mechanical performance.

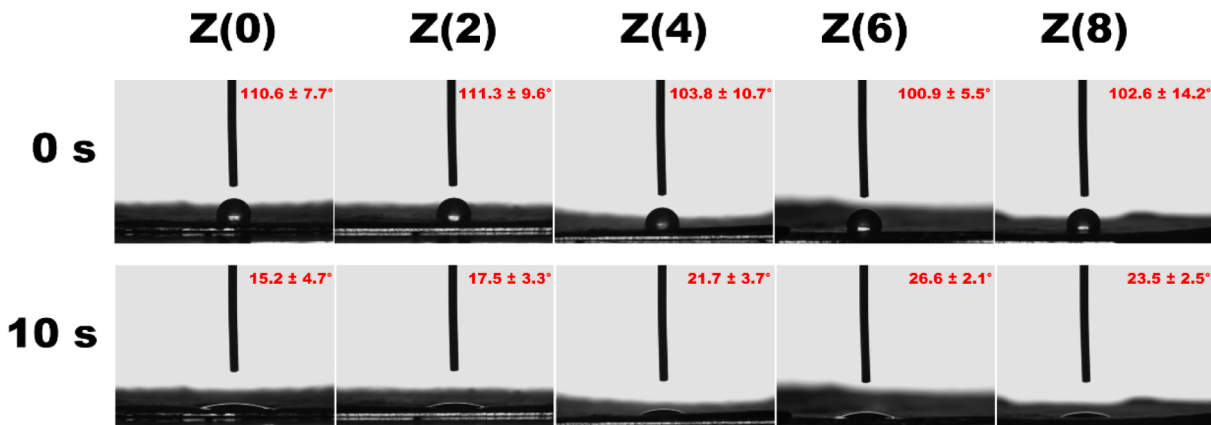


Fig. 5. WCA values of the nanofibers.

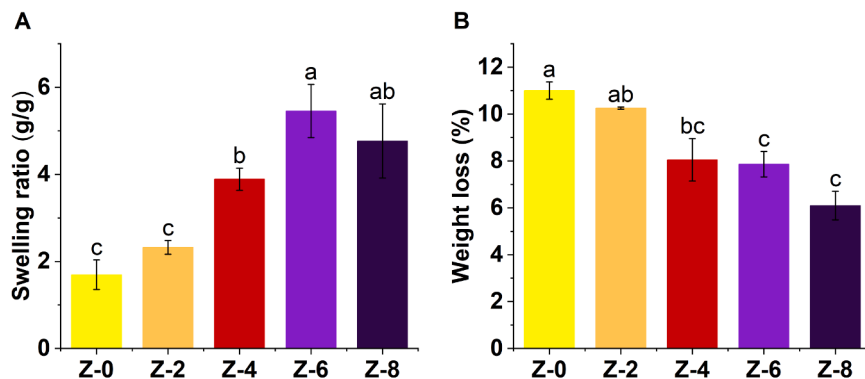


Fig. 6. (A) Swelling ratio and (B) weight loss of the fibers after being immersed in PBS for 25 h. Results with different letters in the same bar chart were significantly different ($P < 0.05$).

The gluten/zein composite nanofibers in the research of Zhang et al. (2022) were crosslinked by β -cyclodextrin, involving the Maillard reaction, and the tensile strength dramatically increased to 13.9 MPa. Therefore, it could be concluded that AD crosslinking contributed to more desirable mechanical performances of the zein nanofiber systems, and a proper amount of AD addition would be beneficial to further

applications.

3.6. WCA

The surface wettability was characterized by WCA and exhibited in Fig. 5. Due to the hydrophilicity of zein and AD, after standing for 10 s, the

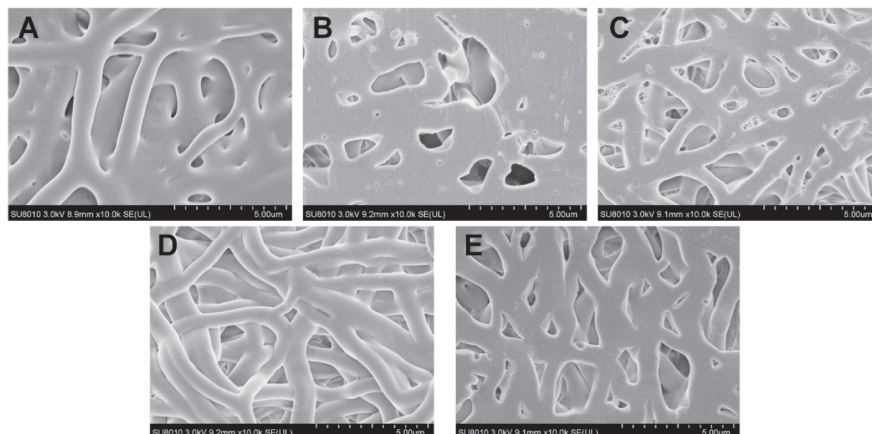


Fig. 7. FE-SEM graphs of the fibers after being immersed in PBS for 25 h. (A) Z-0, (B) Z-2, (C) Z-4, (D) Z-6, and (E) Z-8.

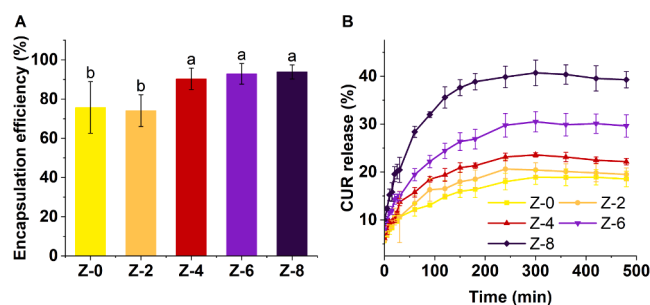


Fig. 8. The encapsulation efficiency (A) and the CUR release profiles (B) of the fibers. Different letters indicated significant differences ($P < 0.05$).

water droplet passed through all the fibrous mats gradually, and the WCA changed from over 100° to below 30° . For the WCA at 10 s, Z-6 and Z-8 presented the highest values: 26.6° and 23.5° , respectively, indicating a high degree of AD crosslinking improved the hydrophobicity of nanofiber mats. This could be explained by the improved compactness of polymer chains due to the incorporation of AD, and the reduction of free hydrophilic groups in fibers (Amjadi et al., 2022). Jia et al. (2022) constructed pea protein isolate composite nanofiber films, and the crosslinking reaction induced by glucose notably increased the WCA of the films. This was because the Maillard reaction consumed the polar groups oriented outward, thereby enhancing the hydrophobicity. But such improvement was limited, as the WCA values were still lower than that of conventional hydrophobic biopolymer-based materials, which were obtained by other strategies (e.g., siliconization using Methyltrimethoxysilane) (Xiao et al., 2021). In addition to the green crosslinking, extra treatments might be supplemented to further optimize the hydrophobicity of the biopolymer materials, such as heating on protein-based nanofibers (Xie et al., 2021).

3.7. Water stability

Pure zein nanofibers had a swelling ratio of 1.70 g/g, and the index went higher as the concentration of AD increased (Fig. 6). Samples with 6 % and 8 % addition of AD owned the highest swelling ratios of 5.45 and 4.76 g/g, respectively, with no significant difference. Meanwhile, the weight loss of the nanofibers decreased continuously from 11.00 % to 6.09 %, with the increasing concentration of AD (Fig. 6B). Such trends could be ascribed to the more compact fibrous structure that favored the retention of water and restricted the liquid phase mobility (Lin, Ni, Liu, Yao, & Pang, 2019). Zhao et al. (2019) reported a nanofiber system made from cellulose and amino acid clusters, where the crosslinking immobilization could promote the absorption and retention of water, resulting in a higher water swelling ratio.

The micrographs of the swelling fibers after being immersed in PBS solutions for 25 h were exhibited in Fig. 7. By the swelling of water, the fibers lost most of their fiber structures and presented adhesive behaviors, but a more obvious fiber morphology could be observed in samples with higher crosslinking degrees (Z-4, Z-6, and Z-8). This might be attributed to the strengthened fiber networks by AD crosslinking that resisted the dissolution and aggregation of fibers (Zhang, Deng, et al., 2022). Such fiber morphology after swelling could also be seen in the study of Wang et al. (2012), where smooth and intact nanofibers with random orientation were retained in the highly crosslinked samples, suggesting excellent water stabilities. Besides, a higher swelling ratio of nanofibers could promote the drug release rate, thus the AD crosslinking would favor the rapid release of active substances to some extent (Deng, Li, Feng, & Zhang, 2019).

3.8. CUR encapsulation efficiency and release behavior

As shown in Fig. 8A, Z-0 possessed an encapsulation efficiency of

Table 3

Fitting parameters from the Korsmeyer-Peppas model for CUR release evaluation.

Sample	<i>k</i>	<i>n</i>	<i>R</i> ²
Z-0	4.52 ± 0.18^c	0.24 ± 0.01^a	0.98
Z-2	4.79 ± 0.23^c	0.25 ± 0.01^a	0.97
Z-4	5.18 ± 0.43^{bc}	0.26 ± 0.02^a	0.95
Z-6	6.23 ± 0.24^b	0.27 ± 0.01^a	0.98
Z-8	8.63 ± 0.69^a	0.28 ± 0.02^a	0.96

Different letters in the same column meant significant difference ($P < 0.05$).

75.73 %, and the 2 % addition of AD (74.11 %) showed no significant influence on the efficiency. When the concentration of AD reached 4 %, the encapsulation efficiency exhibited a significant increase, but the values of Z-4, Z-6, and Z-8 were 90.36 %, 92.91 %, and 93.89 %, respectively, which were statistically identical. The high encapsulation efficiency of highly crosslinked fibers was related to the denser fiber networks, which would favor the protection of loading bioactive substances, such as minimizing the exposure to oxygen (Zhang et al., 2019). In the systems of zein/polyhydroxyalkanoate fibers crosslinked by glutaraldehyde, phenolic extracts could be encapsulated within the fibers effectively, with encapsulation efficiencies from 90.2 % to 94.3 % (Moreno et al., 2019). Such values were considerable and similar to relevant research that encapsulated natural compounds through electrospun zein materials (Alehosseini et al., 2019).

The results of the 8 h release profile of CUR from the fibers were shown in Fig. 8B. The biopolymer fibers would partly dissolve and diffuse in PBS solution, and CUR were rapidly released from the fiber films in the initial 100 min, following the relatively flat stage. Throughout the release process, the films with a higher crosslinking degree presented a higher amount of CUR release. According to the study of Dos Santos et al. (2020), the improved swelling capacity of nanofibers in the aqueous medium was linked with a burst of release as well as a more release amount by diffusion and dissolution of the polymeric matrix, which might account for the effect of AD crosslinking on CUR release. Based on specific conditions, the nanofibers via green crosslinking had promising applications. CUR could be loaded efficiently in Z-8, which was suitable for efficient release applications like nutrition delivery. In addition, the low crosslinking degree may favor the sustained and stable release of active substances (Li, Ding, Yu, Yao, & Boccaccini, 2015).

In addition, different fitting models were used to manifest the release kinetics of CUR. Among the four kinetic models, Korsmeyer-Peppas model showed the highest correlation coefficients (0.95—0.98) and the overall best fitting effect, whose indexes were exhibited in Table 3. With the addition of AD as the crosslinking agent, *k* increased significantly (from 4.52 to 8.63), which directly reflected the improved release rate of CUR. Moreover, *n* of all samples were statistically identical and within the range of 0.223 to 0.303, which indicated that Fickian diffusion dominated the diffusion mechanism of CUR release (Tai et al., 2019). Based on different material systems, the release behavior of CUR may fit with different kinetics models. For instance, Mirzaie, Reisi-Vanani, and Barati (2019) prepared polyvinyl alcohol/graphene oxide (PVA/GO) composite hydrogels for transferring CUR, and decreasing GO content changed the release behavior from Fickian kinetics model to zero order model. In the study of the curcumin-loaded mesoporous silica nanoparticles modified with amine groups, the release behavior was analyzed by the first-order, Weibull, Hixson-Crowell, Korsmeyer-Peppas, and Higuchi models, where Weibull kinetic model was the best fitting (Atiyah, Albayati, & Atiya, 2022).

3.9. Antioxidant activity

CUR owned excellent biological functions, and it was involved as the antioxidant in the manuscript. Considering the limitations of CUR in

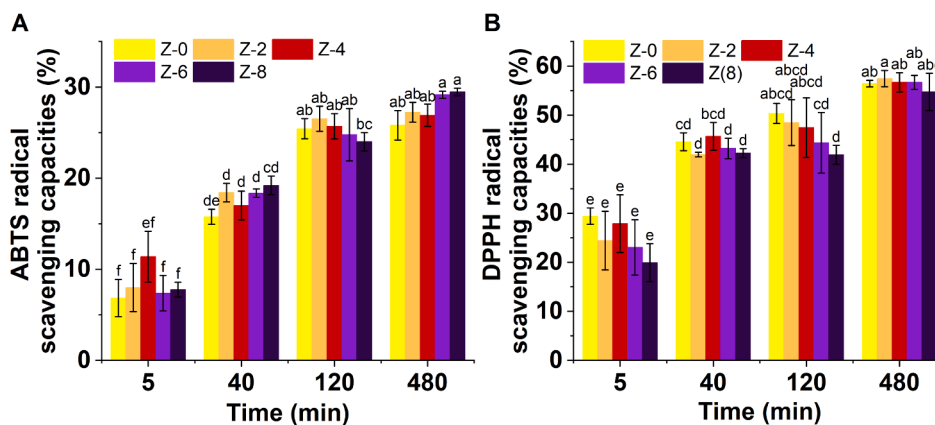


Fig. 9. ABTS (A) and DPPH (B) radical scavenging activities of the fibers. Results without same letters in the same bar chart were significantly different ($P < 0.05$).

food-related and medical areas (poor water solubility and low bioavailability, etc.), it is necessary to investigate the antioxidation during CUR release (Wang et al., 2020). The antioxidant activities of fibers were estimated utilizing the ABTS and DPPH approaches, which were shown in Fig. 9. On the whole, CUR in the fibers was gradually released in the aqueous medium and exerted oxidation resistance, led to increasing ABTS and DPPH values. From 5 to 40 min, the two indexes of each sample increased statistically, but when it came to 120 and 480 min, more changes between adjacent time intervals were of no significance. This was consistent with the CUR release behavior, as a great amount of CUR was released during the initial stage, then the relatively steady stage followed. Specifically, the ABTS radical scavenging activities of all fibers significantly increased from 40 to 120 min, different from DPPH radical scavenging activities with no significance. At 480 min, only the two scavenging activities of Z-8 were significantly improved, as well as the DPPH scavenging activity of Z-6. Besides, five samples displayed no significant difference in the two scavenging activities at the given time. Similar results could be found in other cross-linked biopolymer materials. Bonifacio et al. (2022) constructed gellan gum hydrogels crosslinked by lignin, and the antioxidant features could be explained by lignin content. Pi et al. (2023) crosslinked the soybean protein isolate with proanthocyanidins (PC), where different contents of PC would not alter the ABTS and DPPH radical scavenging activities. Directly adding more active antioxidants (as the crosslinking agent or the loading substance) in the spinning solutions might be the most effective method to improve the oxidation resistance. For instance, Maryam Adilah et al. (2022) used ferulic acid (FA) to crosslink the fish gelatin composite films, and the increasing radical scavenging activity with the increase in FA content proved that FA acted as both the crosslinking agent and the excellent antioxidant. Therefore, the AD-crosslinked zein fibers were expected to perform better antioxidant activities by efficiently encapsulating more CUR.

4. Conclusions

This work developed CUR-loaded and AD-crosslinked zein solutions for electrospinning, and the obtained nanofiber membranes were in different degrees of crosslinking. The crosslinking reaction was proved to occur, and higher degrees of crosslinking enhanced the physical/chemical properties of nanofibers. AD crosslinking led to improved encapsulation efficiency and release rate of CUR, which was relevant to the results of antioxidant abilities. To conclude, a green and facile crosslinking method was applied to fabricate electrospun biopolymer nanofibers. The oxidized polysaccharide was successfully obtained and crosslinked with protein in the electrospun fiber systems. Such formulas could be extended to utilize more saccharides in electrospun nanofiber construction. Furthermore, the release of CUR from nanofibers was

controllable based on different AD crosslinking degrees, suggesting the potential in fabricating loading and delivery materials as per specific requirements.

CRediT authorship contribution statement

Jiawen Li: Writing – review & editing, Writing – original draft, Visualization, Validation, Supervision, Methodology, Investigation, Formal analysis, Data curation. **Yuanhao Zheng:** Writing – original draft, Visualization, Methodology, Investigation, Formal analysis, Data curation. **Peng Wang:** Writing – original draft, Supervision, Software, Methodology, Investigation, Conceptualization. **Hui Zhang:**

Declaration of competing interest

The authors declare that they have no known competing financial interests or personal relationships that could have appeared to influence the work reported in this paper.

Data availability

Data will be made available on request.

Acknowledgment

The research was supported by the Zhejiang Provincial Natural Science Foundation of China for Distinguished Young Scholars (Grant No. LR20C200001), and Zhejiang Provincial Natural Science Foundation of China (Grant No. 2020C02036 and 2021C02032).

References

- Alehosseini, A., Gomez del Pulgar, E.-M., Fabra, M. J., Gómez-Mascaraque, L. G., Benítez-Páez, A., Sarabi-Jamab, M., Ghorani, B., & Lopez-Rubio, A. (2019). Agarose-based freeze-dried capsules prepared by the oil-induced biphasic hydrogel particle formation approach for the protection of sensitive probiotic bacteria. *Food Hydrocolloids*, 87, 487–496. <https://doi.org/10.1016/j.foodhyd.2018.08.032>
- Amjadi, S., Gholizadeh, S., Ebrahimi, A., Almasi, H., Hamishehkar, H., & Taheri, R. A. (2022). Development and characterization of the curcumin-loaded zein/pullulan hybrid electrospun nanofibers for food and medical applications. *Industrial Crops and Products*, 183, Article 114964. <https://doi.org/10.1016/j.indcrop.2022.114964>
- Angarano, M., Schulz, S., Fabritius, M., Vogt, R., Steinberg, T., Tomakidi, P., Friedrich, C., & Mulhaupt, R. (2013). Layered Gradient Nonwovens of In Situ Crosslinked Electrospun Collagenous Nanofibers Used as Modular Scaffold Systems for Soft Tissue Regeneration. *Advanced Functional Materials*, 23(26), 3277–3285. <https://doi.org/10.1002/adfm.201202816>
- Atiyah, N. A., Albayati, T. M., & Atiya, M. A. (2022). Functionalization of mesoporous MCM-41 for the delivery of curcumin as an anti-inflammatory therapy. *Advanced Powder Technology*, 33(2), Article 103417. <https://doi.org/10.1016/j.apt.2021.103417>

- Aydin, S., Kabaoglu, I., Guler, E., Topal, F., Hazar-Yavuz, A. N., Ekentok, C., Tatar, E., Gurbuz, F., Gunduz, O., & Cam, M. E. (2022). A Comparison Study of Fiber Diameter's Effect on Characteristic Features of Donepezil/Curcumin-Loaded Polycaprolactone/Polyactic Acid Nanofibers. *Macromolecular Materials and Engineering*, 307(5), 2100855. <https://doi.org/10.1002/mame.202100855>
- Bonifacio, M. A., Cometa, S., Cochis, A., Scalzone, A., Gentile, P., Scalia, A. C., Rimondini, L., Mastorilli, P., & De Giglio, E. (2022). A bioprintable gellan gum/lignin hydrogel: A smart and sustainable route for cartilage regeneration. *International Journal of Biological Macromolecules*, 216, 336–346. <https://doi.org/10.1016/j.ijbiomac.2022.07.002>
- Campiglio, C. E., Contessi Negrini, N., Fare, S., & Draghi, L. (2019). Cross-Linking Strategies for Electrospun Gelatin Scaffolds. *Materials (Basel)*, 12(15), 2476. <https://doi.org/10.3390/ma12152476>
- Chetouani, A., Elkolloi, M., Haffar, H., Chader, H., Riahi, F., Varacavoudin, T., & Le Cerf, D. (2022). Multifunctional hydrogels based on oxidized pectin and gelatin for wound healing improvement. *International Journal of Biological Macromolecules*, 212, 248–256. <https://doi.org/10.1016/j.ijbiomac.2022.05.082>
- Deng, L., Li, Y., Feng, F., & Zhang, H. (2019). Study on wettability, mechanical property and biocompatibility of electrospun gelatin/zein nanofibers cross-linked by glucose. *Food Hydrocolloids*, 87, 1–10. <https://doi.org/10.1016/j.foodhyd.2018.07.042>
- Deng, L., Zhang, X., Li, Y., Que, F., Kang, X., Liu, Y., Feng, F., & Zhang, H. (2018). Characterization of gelatin/zein nanofibers by hybrid electrospinning. *Food Hydrocolloids*, 75, 72–80. <https://doi.org/10.1016/j.foodhyd.2017.09.011>
- Ding, W., Zhou, J., Zeng, Y., Wang, Y. N., & Shi, B. (2017). Preparation of oxidized sodium alginate with different molecular weights and its application for crosslinking collagen fiber. *Carbohydrate Polymers*, 157, 1650–1656. <https://doi.org/10.1016/j.carbpol.2016.11.045>
- Dos Santos, D. M., Chagas, P. A. M., Leite, I. S., Inada, N. M., de Annunzio, S. R., Fontana, C. R., Campana-Filho, S. P., & Correa, D. S. (2020). Core-sheath nanostructured chitosan-based nonwovens as a potential drug delivery system for periodontitis treatment. *International Journal of Biological Macromolecules*, 142, 521–534. <https://doi.org/10.1016/j.ijbiomac.2019.09.124>
- Drosou, C., Krokida, M., & Biliaderis, C. G. (2018). Composite pullulan-whey protein nanofibers made by electrospinning: Impact of process parameters on fiber morphology and physical properties. *Food Hydrocolloids*, 77, 726–735. <https://doi.org/10.1016/j.foodhyd.2017.11.014>
- Ghasemi, S., Alibaabaei, A., Saberi, R., Esmaeili, M., Semnani, D., & Karbasi, S. (2023). Evaluation of the effects of zein incorporation on physical, mechanical, and biological properties of polyhydroxybutyrate electrospun scaffold for bone tissue engineering applications. *International Journal of Biological Macromolecules*, 253. <https://doi.org/10.1016/j.ijbiomac.2023.126843>
- Hajjari, M. M., Golmakan, M.-T., & Sharif, N. (2023). Electrospun zein/C-phycocyanin composite: Simulation, characterization and therapeutic application. *Food Hydrocolloids*, 140, Article 108638. <https://doi.org/10.1016/j.foodhyd.2023.108638>
- Horuz, T. I., & Belibagli, K. B. (2019). Nanoencapsulation of carotenoids extracted from tomato peels into zein fibers by electrospinning. *Journal of the Science of Food and Agriculture*, 99(2), 759–766. <https://doi.org/10.1002/jsfa.9244>
- Jalaja, K., & James, N. R. (2015). Electrospun gelatin nanofibers: A facile cross-linking approach using oxidized sucrose. *International Journal of Biological Macromolecules*, 73, 270–278. <https://doi.org/10.1016/j.ijbiomac.2014.11.018>
- Jia, X., Li, X., Zhao, J., Kong, B., Wang, H., Liu, Q., & Wang, H. (2022). Fabrication and characterization of crosslinked pea protein isolated/pullulan/allicin electrospun nanofiber films as potential active packaging material. *Food Packaging and Shelf Life*, 33, 100873. <https://doi.org/10.1016/j.jfpsl.2022.100873>
- Laha, A., Sharma, C. S., & Majumdar, S. (2017). Sustained drug release from multi-layered sequentially crosslinked electrospun gelatin nanofiber mesh. *Materials Science & Engineering C-Materials for Biological Applications*, 76, 782–786. <https://doi.org/10.1016/j.mssec.2017.03.110>
- Lertpairrod, J., & Tiyaboonchai, W. (2022). pH-sensitive beads containing curcumin loaded nanostructured lipid carriers for a colon targeted oral delivery system. *Journal of Pharmaceutical Investigation*, 52(3), 387–396. <https://doi.org/10.1007/s40005-022-00572-0>
- Li, J., Zhang, C., Li, Y., & Zhang, H. (2022). Fabrication of aerogel-templated oleogels from alginate-gelatin conjugates for in vitro digestion. *Carbohydrate Polymers*, 291, 119603. <https://doi.org/10.1016/j.carbpol.2022.119603>
- Li, J., & Zhang, H. (2023). Efficient fabrication, characterization, and in vitro digestion of aerogel-templated oleogels from a facile method: Electrospun short fibers. *Food Hydrocolloids*, 135, 108185. <https://doi.org/10.1016/j.foodhyd.2022.108185>
- Li, J., Zhao, S., Zhu, Q., & Zhang, H. (2023). Characterization of chitosan-gelatin cryogel templates developed by chemical crosslinking and oxidation resistance of camellia oil cryogel-templated oleogels. *Carbohydrate Polymers*, 315, 120971. <https://doi.org/10.1016/j.carbpol.2023.120971>
- Li, W., Ding, Y., Yu, S., Yao, Q., & Boccaccini, A. R. (2015). Multifunctional Chitosan-45SS Bioactive Glass-Poly(3-hydroxybutyrate-co-3-hydroxyvalerate) Microsphere Composite Membranes for Guided Tissue/Bone Regeneration. *ACS Applied Materials & Interfaces*, 7(37), 20845–20854. <https://doi.org/10.1021/acsmami.5b06128>
- Lin, W., Ni, Y., Liu, D., Yao, Y., & Pang, J. (2019). Robust microfluidic construction of konjac glucomannan-based micro-films for active food packaging. *International Journal of Biological Macromolecules*, 137, 982–991. <https://doi.org/10.1016/j.ijbiomac.2019.07.045>
- López-Rubio, A., & Lagaron, J. M. (2012). Whey protein capsules obtained through electrospaying for the encapsulation of bioactives. *Innovative Food Science & Emerging Technologies*, 13, 200–206. <https://doi.org/10.1016/j.ifset.2011.10.012>
- Maryam Adilah, Z. A., Han Lyn, F., Nabilah, B., Jamilah, B., Gun Hean, C., & Nur Hanani, Z. A. (2022). Enhancing the physicochemical and functional properties of gelatin/graphene oxide/cinnamon bark oil nanocomposite packaging films using fericulic acid. *Food Packaging and Shelf Life*, 34, 100960. <https://doi.org/10.1016/j.fpsl.2022.100960>
- Mattice, K. D., & Marangoni, A. G. (2021). Physical properties of zein networks treated with microbial transglutaminase. *Food Chemistry*, 338, 128010. <https://doi.org/10.1016/j.foodchem.2020.128010>
- Mendes, A. C., Stephanek, K., & Chronakis, I. S. (2017). Electrospinning of food proteins and polysaccharides. *Food Hydrocolloids*, 68, 53–68. <https://doi.org/10.1016/j.foodhyd.2016.10.022>
- Mirzaie, Z., Reisi-Vanani, A., & Barati, M. (2019). Polyvinyl alcohol-sodium alginate blend, composited with 3D-graphene oxide as a controlled release system for curcumin. *Journal of Drug Delivery Science and Technology*, 50, 380–387. <https://doi.org/10.1016/j.jddst.2019.02.005>
- Moreno, M. A., Orqueda, M. E., Gómez-Mascaraque, L. G., Isla, M. I., & López-Rubio, A. (2019). Crosslinked electrospun zein-based food packaging coatings containing bioactive chilote fruit extracts. *Food Hydrocolloids*, 95, 496–505. <https://doi.org/10.1016/j.foodhyd.2019.05.001>
- Pi, X., Liu, J., Sun, Y., Ban, Q., Liang, S., Cheng, J., & Guo, M. (2023). Effect of proanthocyanidins on protein composition, conformational structure, IgE binding capacities and functional properties in soybean protein. *International Journal of Biological Macromolecules*, 224, 881–892. <https://doi.org/10.1016/j.ijbiomac.2022.10.174>
- Pereira, P., da Cunha, M. D., Ponce, A. G., & Abraham, G. A. (2023). Effect of thermal treatments and UV radiation on green soy protein isolated crosslinked electrospun mats. *Journal of Applied Polymer Science*, 140(17), e53777.
- Singh, B. N., Panda, N. N., & Pramanik, K. (2016). A novel electrospinning approach to fabricate high strength aqueous silk fibroin nanofibers. *International Journal of Biological Macromolecules*, 87, 201–207. <https://doi.org/10.1016/j.ijbiomac.2016.01.120>
- Tai, K., Rappolt, M., He, X., Wei, Y., Zhu, S., Zhang, J., Mao, L., Gao, Y., & Yuan, F. (2019). Effect of β-sitosterol on the curcumin-loaded liposomes: Vesicle characteristics, physicochemical stability, in vitro release and bioavailability. *Food Chemistry*, 293, 92–102. <https://doi.org/10.1016/j.foodchem.2019.04.077>
- Topal, F., Ertas, B., Guler, E., Gurbuz, F., Ozcan, G. S., Aydemir, O., Bocekci, V. G., Duruksu, G., Sahin Cam, C., Yazir, Y., Gunduz, O., & Cam, M. E. (2022). A novel multi-target strategy for Alzheimer's disease treatment via sublingual route: Donepezil/memantine/curcumin-loaded nanofibers. *Biomaterials Advances*, 138, 212870. <https://doi.org/10.1016/j.bioadv.2022.212870>
- Turasan, H., Barber, E. A., Malm, M., & Kokini, J. L. (2018). Mechanical and spectroscopic characterization of crosslinked zein films cast from solutions of acetic acid leading to a new mechanism for the crosslinking of oleic acid plasticized zein films. *Food Research International*, 108, 357–367. <https://doi.org/10.1016/j.foodres.2018.03.063>
- Wang, P., Li, Y., Zhang, C., Feng, F., & Zhang, H. (2020). Sequential electrospinning of multilayer ethylcellulose/gelatin/ethylcellulose nanofibrous film for sustained release of curcumin. *Food Chemistry*, 308, 125599. <https://doi.org/10.1016/j.foodchem.2019.125599>
- Wang, P., Zou, Y., Li, Y., Qin, Z., Liu, X., & Zhang, H. (2022). pH-sensitive self-assembled nanofibers based on electrostatic interaction and Schiff base bonding for controlled release of curcumin. *Food Hydrocolloids*, 131, 107805. <https://doi.org/10.1016/j.foodhyd.2022.107805>
- Wang, S., Cao, X., Shen, M., Guo, R., Banyai, I., & Shi, X. (2012). Fabrication and morphology control of electrospun poly(gamma-glutamic acid) nanofibers for biomedical applications. *Colloids and Surfaces B Biointerfaces*, 89, 254–264. <https://doi.org/10.1016/j.colsurfb.2011.09.029>
- Xiao, W., Wang, P., Song, X., Liao, B., Yan, K., & Zhang, J.-J. (2021). Facile Fabrication of Anisotropic Chitosan Aerogel with Hydrophobicity and Thermal Superinsulation for Advanced Thermal Management. *ACS Sustainable Chemistry & Engineering*, 9(28), 9348–9357. <https://doi.org/10.1021/acssuschemeng.1c02217>
- Xie, X., Li, D., Chen, Y., Shen, Y., Yu, F., Wang, W., Yuan, Z., Morsi, Y., Wu, J., & Mo, X. (2021). Conjugate Electrospun 3D Gelatin Nanofiber Sponge for Rapid Hemostasis. *Advanced Healthcare Materials*, 10(20), e2100918.
- Xu, Y. T., Li, L., Wang, H., Yu, X. X., Gu, Z. P., Huang, C. C., & Peng, H. (2013). In vitro cytocompatibility evaluation of alginate dialdehyde for biological tissue fixation. *Carbohydrate Polymers*, 92(1), 448–454. <https://doi.org/10.1016/j.carbpol.2012.09.096>
- Yao, F., Gao, Y.-H., Chen, F.-S., & Xia, Y.-M. (2021). Effects of electrospinning parameters on peanut protein isolate nanofibers diameter. *CyTA - Journal of Food*, 19(1), 729–738. <https://doi.org/10.1080/19476337.2021.1974950>
- Zhang, C., Li, Y., Wang, P., Zhang, A., Feng, F., & Zhang, H. (2019). Electrospinning of bilayer emulsions: The role of gum Arabic as a coating layer in the gelatin-stabilized emulsions. *Food Hydrocolloids*, 94, 38–47. <https://doi.org/10.1016/j.foodhyd.2019.03.013>
- Zhang, C., Wang, P., Li, J., Zhang, H., & Weiss, J. (2021). Characterization of core-shell nanofibers electrospun from bilayer gelatin/gum Arabic O/W emulsions crosslinked by genipin. *Food Hydrocolloids*, 119, 106854. <https://doi.org/10.1016/j.foodhyd.2021.106854>
- Zhang, Y., Deng, L., Zhong, H., Zou, Y., Qin, Z., Li, Y., & Zhang, H. (2022). Impact of glycation on physical properties of composite gluten/zein nanofibrous films fabricated by blending electrospinning. *Food Chemistry*, 366, 130586. <https://doi.org/10.1016/j.foodchem.2021.130586>
- Zhang, Y., Yang, K., Qin, Z., Zou, Y., Zhong, H., & Zhang, H. (2022). Cross-linked gluten/zein nanofibers via Maillard reaction with the loading of star anise essential oil/

- β -cyclodextrin inclusions for food-active packaging. *Food Packaging and Shelf Life*, 34, 100950. <https://doi.org/10.1016/j.fpsl.2022.100950>
- Zhao, C., Niu, J., Xiao, C., Qin, Z., Jin, X., Wang, W., & Zhu, Z. (2022). Separator with high ionic conductivity and good stability prepared from keratin fibers for supercapacitor applications. *Chemical Engineering Journal*, 444, 136537. <https://doi.org/10.1016/j.cej.2022.136537>
- Zhao, G., Xu, X., Di, Y., Wang, H., Cheng, B., Shi, L., Zhu, Y., Zhuang, X., & Yin, Y. (2019). Amino acid clusters supported by cellulose nanofibers for proton exchange membranes. *Journal of Power Sources*, 438, 227035. <https://doi.org/10.1016/j.jpowsour.2019.227035>